Optics EXPRESS

CMOS compatible fabrication of micro, nano convex silicon lens arrays by conformal chemical vapor deposition

HAIJIE ZUO,[1,2,*] DUK-YONG CHOI,[1] XIN GAI,[1] BARRY LUTHER-DAVIES,[1] AND BAOPING ZHANG[2]

[1]*Laser Physics Centre, The Australia National University, Canberra, ACT 2601, Australia*
[2]*Laboratory of Micro/Nano Optoelectronics, Department of Electronic Engineering, Xiamen University, Xiamen 361005, Fujian, China*
[*]*haijie.zuo@anu.edu.au*

Abstract: We present a novel CMOS-compatible fabrication technique for convex micro-nano lens arrays (MNLAs) with high packing density on the wafer scale. By means of conformal chemical vapor deposition (CVD) of hydrogenated amorphous silicon (a-Si:H) following patterning of silicon pillars via electron beam lithography (EBL) and plasma etching, large areas of a close packed silicon lens array with the diameter from a few micrometers down to a few hundred nanometers was fabricated. The resulting structure shows excellent surface roughness and high uniformity. The optical focusing properties of the lenses at infrared wavelengths were verified by experimental measurements and numerical simulation. This approach provides a feasible solution for fabricating silicon MNLAs compatible for next generation large scale, miniaturized optical imaging detectors and related optical devices.

OCIS codes: (220.4000) Microstructure fabrication; (220.3630) Lenses; (240.3990) Micro-optical devices.

References

1. D. Kang, C. Pang, S. M. Kim, H. S. Cho, H. S. Um, Y. W. Choi, and K. Y. Suh, "Shape-controllable microlens arrays via direct transfer of photocurable polymer droplets," Adv. Mater. **24**(13), 1709–1715 (2012).
2. B. Stoklasa, L. Motka, J. Rehacek, Z. Hradil, and L. L. Sánchez-Soto, "Wavefront sensing reveals optical coherence," Nat. Commun. **5**, 3275 (2014).
3. Y. M. Song, Y. Xie, V. Malyarchuk, J. Xiao, I. Jung, K. J. Choi, Z. Liu, H. Park, C. Lu, R. H. Kim, R. Li, K. B. Crozier, Y. Huang, and J. A. Rogers, "Digital cameras with designs inspired by the arthropod eye," Nature **497**(7447), 95–99 (2013).
4. G. Agranov, V. Berezin, and R. H. Tsai, "Crosstalk and microlens study in a color CMOS image sensor," IEEE Trans. Electron Dev. **50**(1), 4–11 (2003).
5. J. Lim, P. Gruner, M. Konrad, J.-C. Baret, A. B. Theberge, F. Courtois, Y. Schaerli, M. Fischlechner, and D. D. C. Bradley, "Micro-optical lens array for fluorescence detection in droplet-based microfluidics," Lab Chip **13**(8), 1472–1475 (2013).
6. W. Choi, R. Shin, J. Lim, and S. Kang, "Design methodology for a confocal imaging system using an objective microlens array with an increased working distance," Sci. Rep. **6**, 33278 (2016).
7. X. Xiao, B. Javidi, M. Martinez-Corral, and A. Stern, "Advances in three-dimensional integral imaging: sensing, display, and applications [Invited]," Appl. Opt. **52**(4), 546–560 (2013).
8. M. Thomschke, S. Reineke, B. Lüssem, and K. Leo, "Highly efficient white top-emitting organic light-emitting diodes comprising laminated microlens films," Nano Lett. **12**(1), 424–428 (2012).
9. E. K. Kang, Y. M. Song, S. J. Jang, C. Il Yeo, and Y. T. Lee, "Increased light extraction from GaN Light-emitting diodes by SiN x compound eyes," IEEE Photonics Technol. Lett. **25**(12), 1118–1121 (2013).
10. Y. Chen, M. Elshobaki, Z. Ye, J.-M. Park, M. A. Noack, K.-M. Ho, and S. Chaudhary, "Microlens array induced light absorption enhancement in polymer solar cells," Phys. Chem. Chem. Phys. **15**(12), 4297–4302 (2013).
11. J. D. Myers, W. Cao, V. Cassidy, S.-H. Eom, R. Zhou, L. Yang, W. You, J. Xue, P. Peumans, and A. Yakimov, "A universal optical approach to enhancing efficiency of organic-based photovoltaic devices," Energy Environ. Sci. **5**(5), 6900 (2012).
12. J. Lim, J. Vrignon, P. Gruner, C. S. Karamitros, M. Konrad, and J. C. Baret, "Ultra-high throughput detection of single cell β-galactosidase activity in droplets using micro-optical lens array," Appl. Phys. Lett. **103**(20), 203704 (2013).

#281072 https://doi.org/10.1364/OE.25.003069
Journal © 2017 Received 17 Nov 2016; revised 26 Jan 2017; accepted 1 Feb 2017; published 6 Feb 2017

Optics EXPRESS

13. J. Lim, P. Gruner, M. Konrad, and J.-C. Baret, "Micro-optical lens array for fluorescence detection in droplet-based microfluidics," Lab Chip **13**(8), 1472–1475 (2013).
14. M. B. Stern, "Binary optics: A VLSI-based microoptics technology," Microelectron. Eng. **32**(1–4), 369–388 (1996).
15. Y. Kumaresan, A. Rammohan, P. K. Dwivedi, and A. Sharma, "Large area IR microlens arrays of chalcogenide glass photoresists by grayscale maskless lithography," ACS Appl. Mater. Interfaces **5**(15), 7094–7100 (2013).
16. H. Jung and K.-H. Jeong, "Monolithic polymer microlens arrays with high numerical aperture and high packing density," ACS Appl. Mater. Interfaces **7**(4), 2160–2165 (2015).
17. H. Toshiyoshi, G. D. J. Su, J. LaCosse, and M. C. Wu, "A surface micromachined optical scanner array using photoresist lenses fabricated by a thermal reflow process," J. Lightwave Technol. **21**(7), 1700–1708 (2003).
18. Z. Deng, Q. Yang, F. Chen, X. Meng, H. Bian, J. Yong, C. Shan, and X. Hou, "Fabrication of large-area concave microlens array on silicon by femtosecond laser micromachining," Opt. Lett. **40**(9), 1928–1931 (2015).
19. X. Li, H. Tian, Y. Ding, J. Shao, and Y. Wei, "Electrically templated dewetting of a UV-curable prepolymer film for the fabrication of a concave microlens array with well-defined curvature," ACS Appl. Mater. Interfaces **5**(20), 9975–9982 (2013).
20. X. Li, Y. Ding, J. Shao, H. Tian, and H. Liu, "Fabrication of microlens arrays with well-controlled curvature by liquid trapping and electrohydrodynamic deformation in microholes," Adv. Mater. **24**(23), OP165 (2012).
21. M. Khorasaninejad, W. T. Chen, R. C. Devlin, J. Oh, A. Y. Zhu, and F. Capasso, "Metalenses at visible wavelengths: Diffraction-limited focusing and subwavelength resolution imaging," Science **352**(6290), 1190–1194 (2016).
22. A. Arbabi, Y. Horie, A. J. Ball, M. Bagheri, and A. Faraon, "Subwavelength-thick lenses with high numerical apertures and large efficiency based on high-contrast transmitarrays," Nat. Commun. **6**, 7069 (2015).
23. L. Lin, X. M. Goh, L. P. McGuinness, and A. Roberts, "Plasmonic lenses formed by two-dimensional nanometric cross-shaped aperture arrays for Fresnel-region focusing," Nano Lett. **10**(5), 1936–1940 (2010).
24. H. Gao, J. K. Hyun, M. H. Lee, J. C. Yang, L. J. Lauhon, and T. W. Odom, "Broadband plasmonic microlenses based on patches of nanoholes," Nano Lett. **10**(10), 4111–4116 (2010).
25. L. F. Peng, Y. J. Deng, P. Y. Yi, and X. M. Lai, "Micro hot embossing of thermoplastic polymers: a review," J. Micromech. Microeng. **24**(1), 013001 (2014).
26. N. Guo, W. D. Hu, X. S. Chen, C. Meng, Y. Q. Lv, and W. Lu, "Optimization of Microlenses for InSb Infrared Focal-Plane Arrays," J. Electron. Mater. **40**(8), 1647–1650 (2011).
27. IR camera ImageIR 10300 Serie "InfraTec," http://www.infratec.eu/thermography/infrared-camera/imageirr-10300-series.html.
28. R. Fontaine, "Innovative technology elements for large and small pixel CIS devices," Proc. IISW. 1–4 (2013).
29. E. Markweg, M. Hillenbrand, S. Sinzinger, and M. Hoffmann, "Planar plano-convex microlens in silica using ICP-CVD and DRIE," Proc. SPIE **8550**, 85500T (2012).
30. Z. Deng, F. Chen, Q. Yang, H. Bian, G. Du, J. Yong, C. Shan, and X. Hou, "Dragonfly-eye-inspired artificial compound eyes with sophisticated imaging," Adv. Funct. Mater. **26**(12), 1995–2001 (2016).
31. X. Gai, D. Y. Choi, and B. Luther-Davies, "Negligible nonlinear absorption in hydrogenated amorphous silicon at 1.55 μm for ultra-fast nonlinear signal processing," Opt. Express **22**(8), 9948–9958 (2014).
32. J. S. Pelc, K. Rivoire, S. Vo, C. Santori, D. A. Fattal, and R. G. Beausoleil, "Picosecond all-optical switching in hydrogenated amorphous silicon microring resonators," Opt. Express **22**(4), 3797–3810 (2014).
33. O. Graydon, "Silicon photonics: Amorphous alternative," Nat. Photonics **6**(11), 716 (2012).
34. H. H. Li, "Refractive index of silicon and germanium and its wavelength and temperature derivatives," J. Phys. Chem. Ref. Data **9**(3), 561–658 (1980).
35. Y. O. Yan, B. T. Chen, F. H. Tay, and C. Lliescu, "Process analysis and optimization on PECVD amorphous silicon on glass substrate," J. Phys. Conf. Ser. **34**(1), 812–817 (2006).
36. Lumerical Solutions, Inc., "Innovative Photonic Design Tools," https://www.lumerical.com/
37. R. Stanley, "Plasmonics in the mid-infrared," Nat. Photonics **6**(7), 409–411 (2012).

1. Introduction

Microlens arrays have been commonly incorporated in a variety of optical systems for optical sensors [1–6], 3D displays [7], lighting and photovoltaic devices [8–11], as well as in optofluidic lab-on-a-chip devices [12, 13]. During the past decades, enormous effort has been devoted to developing new methods of fabricating various kinds of microlens arrays, such as the VLSI-based binary method [14]; greyscale lithography [15]; polymer reflow [9,16,17]; femtosecond laser micromachining [18]; electrically templated de-wetting [19,20]; and most recently, planar metamaterial focusing [21,22] and plasmonic focusing [23,24], etc. Among these methods, thermal polymer reflow has been the most widely used as it is compatible with standard semiconductor processes and the lens curvature can be defined by a properly regulated temperature. This approach, however, suffers from the following drawbacks. Firstly, almost all polymers have high absorption in the infrared band, thus hindering their applications in infrared optics. Moreover, it is very difficult to form microlens array with high

Optics EXPRESS

filling factor and a stable curvature over a large area due to merging of neighboring droplets and volumetric shrinkage caused by thermally induced liquid evaporation. As a result the method is not suitable for forming lens arrays at the sub-micron or even the nanometer scale [25]. In some cases where extremely low temperature is required, the stress between the polymer layer and the substrate can cause cracking and deformation, thus limiting its applications in cooled detectors [26,27]. Additionally, most of alternative methods requires sophisticated processes and suffer from low yield, which is not compatible with modern CMOS process, thus it is hard to ensure high yield whilst remaining cost-effective.

Apart from being a major semiconductor material, silicon is also an excellent optical material in the near and mid-infrared due to its broad mid-IR transparency and mechanical stability. Silicon microlens has long been a highly desirable device for various infrared optical devices, and are deemed as a vital component for next generation charge-coupled devices (CCDs) with a pitch down to one or two times of operating wavelength [27,28]. Currently silicon microlenses with a curved surface can only be manufactured via plasma etching with thermally formed polymer microlens as the etch mask, and these suffer from the fundamental hurdles stated above. Markweg *et al* [29] proposed a novel approach by engineering the refractive index in the vertical direction whilst creating a geometrical profile in the orthogonal direction parallel to the substrate. This allowed the beam to be focused along the propagation axis. This method is used for planar beam shaping in chip scale integration within the substrate. Until recently high quality silicon microlens arrays were fabricated by laser enhanced wet etching [18,30]; unfortunately this method can only be used to fabricate concave lens structures, which implies limited application in optical devices compared to the convex counterpart.

In this letter we report a simple, yet efficient method for generating large scale, high quality, convex microlens arrays by CMOS compatible processes with the lens size ranging from several microns to as small as several hundred nanometers. This method consists of two essential steps. First, plasma etching following lithography was used to define the position and "seed" structure of MNLAs on a silicon wafer. As a result an array of silicon pillars was patterned where the pillar structure was predesigned according to the desired lens structure. Second, plasma-enhanced CVD of a-Si:H was performed for conformal growth of MNLAs. The simplicity and cost-effectiveness of the approach could lead to wide applications in next generation high resolution imaging detectors.

2. Experimental Details

2.1 Chemicals and material

Hydrogenated amorphous silicon (a-Si:H) is widely used in photonic applications such as waveguides, photonic crystals and related integrated optical devices because it can be deposited at relatively low temperature on almost any substrate and has comparable optical transmission to crystalline silicon (c-Si) [31–33]. The existence of narrow absorption peaks (FWHM~0.1μm) of Si-H/Si-H_2 at 5μm in a-Si:H has only a minor effect on the overall performance of MNLAs required for wide band focusing within the infrared atmospheric window. Here, a-Si:H was used to build the MNLAs because it exhibits similar refractive index ($\Delta n<0.1$ @1.5μm~10μm, see Fig. 1) to c-Si [34] and this is crucial to enhance light throughput by reducing the Fresnel reflection at the interface between deposition layer and substrate template. Moreover, low temperature deposition by PECVD, a standard CMOS compatible process, can mitigate the thermal stress between a-Si:H and c-Si because of their different thermal expansion coefficients. The deposition rate using our recipe was 20nm/min for a PECVD tool designed for R&D, however, the typical deposition rate in tools used for production is higher ranging from 100~200nm/min [35], which means these lens structures can be created reasonably rapidly.

We, firstly, developed a deposition recipe for a-Si:H films that led to a smooth surface with the lowest optical attenuation based on our previous work [31]. As we can see from Fig.

Optics EXPRESS

1, a-Si:H deposited in optimized conditions shows a negligible extinction coefficient (<0.001, measured by IR-VASE, JA Woollam, Inc.) over the wavelength range from 1.5 µm all the way down to 10 µm. Compared to our previous work, the deposition temperature was reduced from 250°C to 200 °C to mitigate the compressive thermal stress between a-Si:H layer and c-Si substrate.

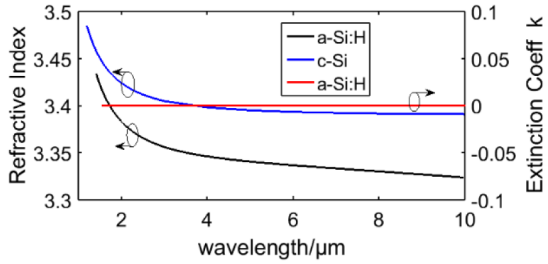

Fig. 1. The index of refraction and extinction coefficients of a-Si:H film grown by PECVD of 2 µm thickness. For comparison, refractive index of c-Si is added [33].

2.2 Experiment procedure

The overall procedure for fabricating the MNLAs is shown schematically in Fig. 2, and mainly consists of two parts: silicon template fabrication [Figs. 2(a)–2(d)] and a-Si:H deposition [Figs. 2(e)–2(f)]. Firstly, a two dimensional periodic array pattern was defined by electron beam lithography (EBL, Raith150) using a positive resist, ZEP 520A, and 70 nm of chromium (Cr) was deposited on top by electron beam evaporation (Temescal BJD-2000). Then, the resist was dissolved in resist remover (ZDMAC from ZEON Co.), leaving a patterned mask of Cr metal. Finally, a template consisting of silicon pillars was obtained by vertical etching the silicon by inductively-coupled-plasma reactive ion etching (ICP-RIE, Oxford Plasmalab System 100) using CHF_3 and SF_6 gas mixture. The residual Cr was removed by immersing the sample in chromium etchant (CR-7 from Cyantek). The inset next to Fig. 2(d), shows a scanning electron micrograph of the resulting c-Si pillar array where the structure parameters such as diameter and height were predesigned according to the MNLAs structure that was required. a-Si:H was then deposited onto the silicon template using the PECVD. In the initial stage of deposition [Fig. 2(e)], the a-Si:H was mainly deposited on the top surface of the silicon pillars and the other horizontal surfaces. As the deposition continued, a-Si:H gradually cover the pillars in a conformal manner such that the deposition rate becomes substantially the same in all directions. Thus, the "lens" diameter increases as the deposition proceeds until the lateral diameter reaches that of the lattice pitch [Fig. 2(f)]. Then the lens boundaries begin to overlap and the overall surface merges to form a continuous corrugated honeycomb structure and the fill factor increases to 100% [Fig. 2(g)]. In this way we could obtain individual isolated hemispheres, as well as closely packed micro or nano dome structures.

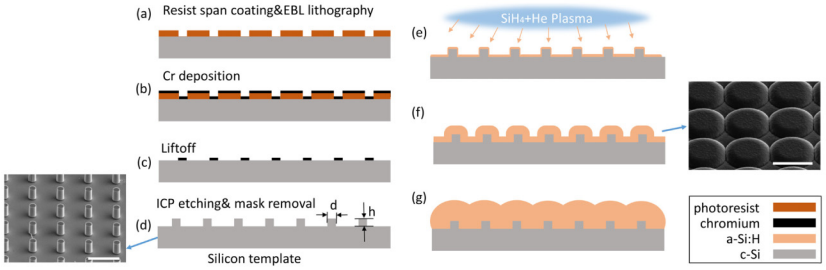

Fig. 2. Schematic of microlens fabrication procedure. Inset: (d): SEM image of silicon template, (f): isolated hemispheres. Scale bar: 5 µm.

Optics EXPRESS

3. Results and discussion

Different pillar array structures could be designed in order to obtain microlenses with particular shapes. The detailed relation between the evolution of the surface profile and a-Si:H deposition onto specific initial pillar structure is rather complex, and is being carefully studied using molecular dynamics models by Monte-Carlo method and deposition experiments, but this is beyond the scope of this paper. However, a linear dependence between lens radius and deposition thickness can be deduced by studying the cross-section, and is discussed in detail in the following part. It is clear that the lattice size and pitch of the MNLAs is defined by that of the c-Si pillars, whilst the radius of each lens generally increases as the thickness of the deposited film increases, which leads to an increasing focal length.

3.1 Nanolens array overgrowth

The EBL and the lift off process were used to define nano pillars on a silicon template. The diameter of the pillars, d, was nominally 200 nm, and the pillar height, h, was 200 nm. Typical SEM image of the silicon nano pillar template is shown in Fig. 3(a). Because of proximity effect during EBL exposure, pillars with different diameters were obtained in a single array depending on the relative position of each pillar. Thus, the diameter of the silicon pillars near the boundary was 200 nm, while those located near the center had a smaller diameter closer to 70 nm. After depositing 800 nm of a-Si:H, a nano lens array with good surface quality was obtained, as shown in the SEM image of Fig. 3(b). The final lens diameter was completely defined by the template so that the lenses near the boundary were larger than those in the central area. The structure shows high fidelity to the templates and demonstrates the feasibility of this overgrowth process.

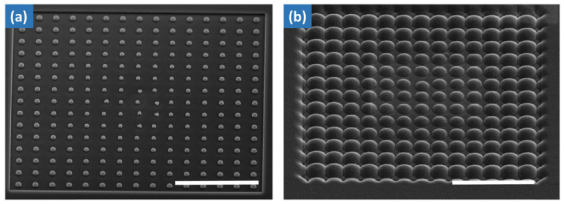

Fig. 3. Nano lens array formation. (a) SEM image of nano-pillar template, (b) nano lens array after overgrowth, tilted 45°, Scale bar: 5 μm.

3.2 Microlens array overgrowth

Microlens arrays with different lattice type and pitch were designed and fabricated. At this scale the period of pillars is at the micron level and was not affected by the proximity effect, thus all the pillar templates had the same diameter within each array, as is depicted in the inset in Fig. 2(d), as a result all the microlens array had uniform size distribution. Hexagonal and rectangular lattices were patterned and three different pitches of 4, 8, and 12 μm were designed for each lattice type in order to obtain lens arrays with various unit cell size. The pillar diameter and height were set to be 1 μm and 2 μm, respectively. The obtained microlens arrays with 4 μm pitch are shown in Figs. 4(a)-4(d), for the different lattice types and deposition thickness. After 3μm of a-Si:H deposition, the lens structure takes up most of the space between the pillars, and the outermost boundaries begin to overlap, increasing the fill factor close to 100%. With further a-Si:H deposition, Figs. 4(c) and 4(d), the space between these micro-domes begins to disappear thus forming microlens structures with 100% fill factor. The radius of curvature of each lenslet increased as the deposition progressed, and the MLAs exhibit high uniformity. We verified that the lens surface has a root-mean-square roughness below 20nm from measurements using Wyko NT9100 optical profiler; however, this roughness would incur only marginal surface scattering at least in the mid infrared range.

Optics EXPRESS

Microlens arrays with larger pitch were also characterized. Figure 5 shows MLAs with 8 µm and 12 µm pitch under high magnification where the a-Si:H deposition thickness was 5 µm. Focused Ion Beam (FIB, FEI Helios 600 NanoLab) milling was used to investigate the cross-sectional profile of an isolated lens structure. As is evident from the FIB cross-section [Fig. 5(g)], the boundary of the deposited layer can be clearly seen and has a spherical shape with smooth surface. When a microlens is isolated, i.e., the radius of the individual lens is smaller than the pitch and the structure of all the microlenses remained the same regardless of the lattice type and pitch. As we can see in Fig. 5(g), the thickness over the curved region of the lens (Δt_1) is equal to that on the plane surface nearby (Δt_2), which indicates that the deposition was conformal. The radius increment ΔR depends linearly on the deposition thickness Δt. One can fit this linear dependence using measured data points (for template pillar d = 1 µm and h = 2 µm, and this results in the relation $R = 0.49 \times t + 1.35$, where R is the radius and t is the deposition thickness). This linear relation can be applied for other templates where different pillar structures are used. After a certain deposition thickness, the lens radius reaches to a point where lens boundary begins to overlap with its neighbors (i.e. Figure 4), the lens radius in this deposition regime can be fully controlled by the designed templates (equals to half of lattice constant). This structure is always preferred in practical applications as it can achieve a 100% fill factor.

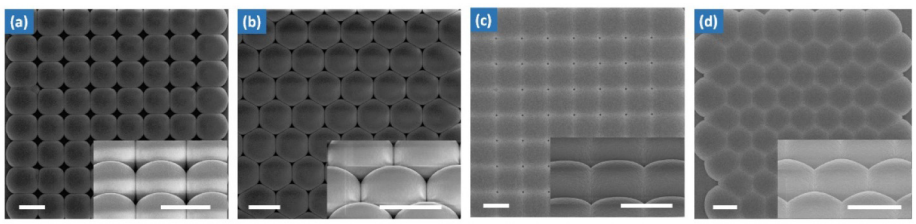

Fig. 4. Microlens array with different lattice and deposition thickness. (a) Rectangular and (b) hexagonal array with 3µm deposition. (c) Rectangular and (d) hexagonal, 5 µm. Insets shows 45° tilted view from SEM. Scale bar 4 µm.

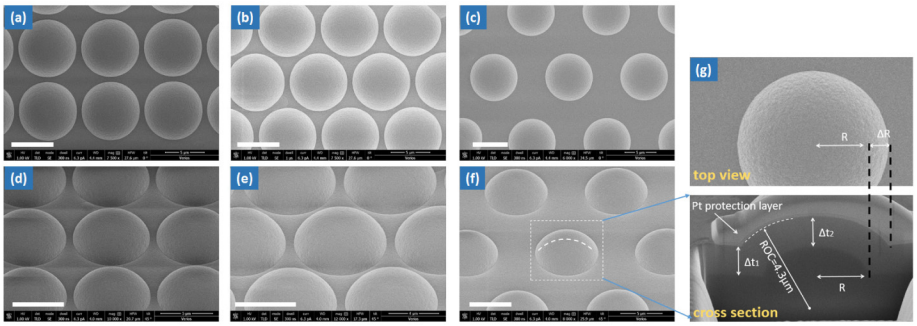

Fig. 5. Detailed view of selected MLAs with larger pitch. (a), (d) rectangular lattice, pitch: 8µm; (b), (e) hexagonal lattice, pitch: 8 µm; (c), (f) hexagonal lattice, pitch: 12 µm, (g) top view and cross section by FIB. (a-c) vertical angle, (d-f) tilted 45°. Scale bar: 5 µm.

The optical performance of close-packed MLAs was characterized using the setup shown in Fig. 6(a). Amplified spontaneous emission (ASE) from an erbium-doped fiber amplifier (EDFA) was utilized as the illumination source as it produces less speckle and a relatively uniform power pattern in the image plane compared with coherent sources. The objective lens was anti-reflection coated for 1550 nm and the image was captured by an InGaAs infrared camera (Xenics, Xeva-1.7-320). Figures 6(b) and 6(c) illustrate the focal spot array of short band ASE centered at 1550 nm. An array of bright spots was observed with high spatial resolution. For a hexagonal lattice with 8 µm pitch, the full width at half-maximum (FWHM)

Optics EXPRESS

of the point spread function (PSF) was fitted to be 2.1 μm at 1550 nm incidence, corresponding to 1.35 times the wavelength. We expect the actual FWHM should be smaller, considering the limited resolution of the tube-lens used in the measurement system and numerical aperture (NA) mismatch between individual microlens unit (~2.9) and imaging objective lens (0.80). The transmitted light intensity of the lens array reached 85% of that of un-patterned flat surface. This indicates that only marginal extra loss is added presumably due to a-Si:H absorption and surface scattering.

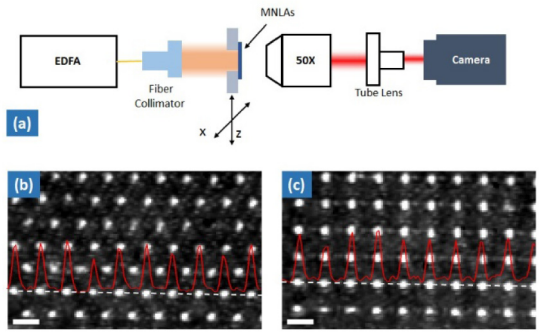

Fig. 6. (a) Schematic of optical measurement system. Focal spot array of ASE from EDFA, (b) hexagonal and (c) rectangular array. Scale bar: 8 μm.

The broad transparency of a-Si:H in the infrared could also make the lenses useful in the mid-infrared (MIR). Currently the resolution of optics used in the MIR in our laboratory is not enough to distinguish between the array of focal spots from those caused by the interference patterns caused by the periodic array. Instead we applied the highly accurate finite-difference time-domain (FDTD from Lumerical, Vancouver) [36] method to calculate the focal response of the MLAs in the MIR. The calculated results confirmed the focusing ability of MLAs, as shown in Fig. 7 where the structural parameter was taken from Fig. 5(g) with a numerical aperture around 2.9. We obtained a sub-wavelength focus reaching FWHM about 0.84 μm, which is close to the diffraction-limited (0.69 μm). Note that the pixel pitch of the most state-of-the-art commercial MIR cameras has been reduced to about two wavelength (~10 μm) [27]. As a result the microlens array could be used to decrease the cross-talk and increase the detectivity. Moreover the high NA and the diffraction-limited focal spot can also make it possible to achieve smaller pixel pitch thus leading to a higher resolution comparable to the more highly developed visual and NIR counterparts [4, 28]. The microlens array might also find applications in MIR plasmonics where high intensity localized electromagnetic field is preferred [37].

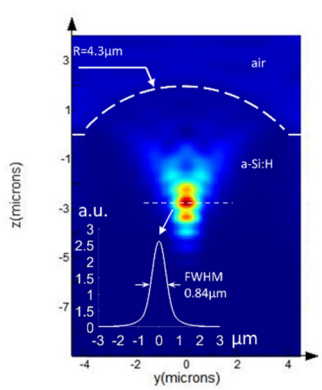

Fig. 7. The FDTD simulation showing the focal property of microlens array at 4μm incidence.

Optics EXPRESS

4. Conclusion

In summary, we presented a novel CMOS compatible, mass producible approach to fabricating convex lens arrays on a silicon substrate. The structure was characterized by SEM and FIB and showed high surface quality and uniformity. Lens arrays with the size of several microns down to several hundred nanometers can be easily fabricated over large areas with high surface quality and uniformity with 100% fill factor. The relation between the lenses radius and the deposition thickness was discussed. It was also verified that the fabricated microlens array produces high resolution and uniform focal spot arrays at 1550 nm. Furthermore, the focusing effect of the MLAs in the MIR (4 μm) was confirmed by FDTD calculations. Due to the high transmission at broad wavelength band, this kind of micro-optical devices promises wide application in next generation high resolution infrared imaging, displays and other related fields. Besides, the excellent mechanical property of a-Si:H renders the silicon convex lens arrays to be used as mold for polymer microlens imprinting.

Funding

China Scholarship Council (201506310074); Australian Research Council (ARC) Future Fellowship (FT110100853); ARC Centre of Excellence for Ultrahigh Bandwidth Devices for Optical Systems (CE110001018).

Acknowledgments

The authors acknowledges the facility support from the ANU node of the Australian National Fabrication Facility (ANFF). We are also thankful to Dr. Steve Madden for helpful discussions in terms of optical measurement.